Nuclear structure in the vicinity of $N = Z = 28$ ^{56}Ni

K. L. Yurkewicz,[1,2] D. Bazin,[2] B. A. Brown,[1,2] C. M. Campbell,[1,2] J. A. Church,[1,2]
D.-C. Dinca,[1,2] A. Gade,[1,2] T. Glasmacher,[1,2] M. Honma,[3] T. Mizusaki,[4]
W. F. Mueller,[2] H. Olliver,[1,2] T. Otsuka,[5,6] L. A. Riley,[7] and J. R. Terry[1,2]

[1]*Department of Physics and Astronomy, Michigan State University, East Lansing, MI 48824*
[2]*National Superconducting Cyclotron Laboratory, Michigan State University, East Lansing, MI 48824*
[3]*Center for Mathematical Sciences, University of Aizu, Tsuruga, Ikki-machi, Aizu-Wakamatsu, Fukushima 965-8580, Japan*
[4]*Institute of Natural Sciences, Senshu University, Higashimita, Tama, Kawasaki, Kanagawa 214-8580, Japan*
[5]*Department of Physics and Center for Nuclear Study, University of Tokyo, Hongo, Tokyo 113-0033, Japan*
[6]*RIKEN, Hirosawa, Wako-shi, Saitama 351-0198, Japan*
[7]*Department of Physics and Astronomy, Ursinus College, Collegeville, PA 19426*

(Dated: September 21, 2004)

Abstract

The isotopes ^{54}Ni, ^{56}Ni and ^{58}Ni have been studied via intermediate-energy Coulomb excitation at the National Superconducting Cyclotron Laboratory. Absolute $B(E2; 0_1^+ \rightarrow 2_1^+)$ excitation strengths have been determined for all three nuclei using a consistent experimental approach, and a measure of quadrupole collectivity has been established in the vicinity of the much discussed doubly–magic shell closure at $N = Z = 28$. The energy of and excitation strength to the first 2^+ state of ^{54}Ni have been observed for the first time. The results are compared to large–scale shell–model calculations that predict that the $E2$ strength in ^{54}Ni should be divided between the first and second 2^+ states.

PACS numbers: 25.70.De, 27.40.+z
Keywords: Intermediate–energy Coulomb excitation, ^{54}Ni, ^{56}Ni, ^{58}Ni

In the nuclear shell model, the first shell closure beyond the harmonic oscillator magic numbers, essentially created by the inclusion of the spin–orbit force, is 28. The self-conjugate nucleus ^{56}Ni, with $N = Z = 28$, is the lightest *exotic* doubly–magic nucleus and the heaviest doubly–magic $N = Z$ nucleus accessible to in-beam γ–ray spectroscopy at existing rare–isotope facilities. Discoveries of phenomena such as "the island of inversion" [1] and the breakdown of the $N = 28$ magic shell closure in ^{44}S [2–5] have demonstrated that the shell structure of exotic nuclei beyond the valley of β stability can be significantly modified compared to stable species.

^{56}Ni has attracted much attention in recent years, both from an experimental and theoretical point of view. A high excitation energy of the first 2^+ state and a low $B(E2; 0_1^+ \rightarrow 2_1^+)$ quadrupole excitation strength within an isotopic chain are generally assessed as necessary signatures for a shell closure. The energy of the 2_1^+ state in ^{56}Ni is well known and with $E(2_1^+) = 2701$ keV significantly higher than the corresponding observable $E(2_1^+) = 1454$ keV in the heavier even–even neighbor ^{58}Ni. The determination of the $B(E2; 0_1^+ \rightarrow 2_1^+)$ excitation strength in ^{56}Ni has been addressed with a variety of experimental methods. In 1973 a lifetime measurement using the Doppler–shift attenuation method yielded $B(E2\uparrow) = 385(160)\ e^2\text{fm}^4$ [6]. More recently, a proton scattering experiment [7] and an intermediate–energy Coulomb excitation measurement [8] indicated with surprisingly high values of $B(E2\uparrow) = 600(120)\ e^2\text{fm}^4$ and $B(E2\uparrow) = 580(70)\ e^2\text{fm}^4$, respectively, a possible change in the behavior of ^{56}Ni compared to stable doubly–magic nuclei.

The aim of the present study is to track the evolution of collectivity in the chain of even mass Ni isotopes with $26 \leq N \leq 30$ using a consistent approach for all three isotopes of interest, projectile Coulomb excitation at intermediate beam energies.

Intermediate–energy Coulomb excitation is a well established and widely used experimental technique used to probe nuclear structure, especially the aspect of quadrupole collectivity in even–even nuclei far from stability [9, 10]. Radioactive nuclei are scattered off stable high–Z targets and are detected in coincidence with the de–excitation γ rays tagging the inelastic process (see for example [9, 11, 12]).

While in Coulomb–excitation experiments at sub–barrier energies nuclear contributions to the excitation process are widely excluded, in the intermediate–energy regime very peripheral collisions have to be selected to ensure a dominance of the electromagnetic interaction. In the present experiments this is accomplished by restricting the analysis to scattering events at extremely forward scattering angles, which correspond to large impact parameters.

The experiments on the Ni isotopes were performed at the Coupled Cyclotron Facility [13] of the NSCL at Michigan State University. The primary beam of ^{58}Ni was accelerated to 140 MeV/nucleon in the K500 and K1200 cyclotrons, and impinged on a thick ^{9}Be fragmentation target to produce the secondary beams of the different Ni isotopes. Characteristics of the fragment beams are listed in Table I. The large–acceptance A1900 fragment separator [14] was used to select the secondary beams.

SeGA [15], an array of 18 32–fold segmented high purity germanium detectors, was used to tag the inelastic process via γ–ray spectroscopy. The high-resolution S800 spectrograph [16, 17] was used in conjunction with SeGA to identify the particles and reconstruct their scattering angle on an event–by–event basis. Details of the experimental setup and the determination of the scattering angle using the S800 focal-plane detector system have been previously discussed [11, 18]. The magnetic spectrograph was operated in dispersion-matched optics mode.

The ^{197}Au Coulomb excitation target was placed at the center of SeGA. The high degree

TABLE I: Secondary beam characteristics for Coulomb excitation experiments. Given are the thicknesses of the production and Coulomb–excitation targets, the energy before the Au target and the approximate intensity at the target position of the S800 spectrograph. The primary beam was ^{58}Ni at 140 MeV/nucleon. The Be target used in the case of the secondary beam ^{58}Ni served as a degrader in energy.

	^{58}Ni	^{56}Ni	^{54}Ni
^{9}Be Production Target (mg/cm^2)	790	423	376
^{197}Au Target (mg/cm^2)	184.1	184.1	257.7
Energy (MeV/nucleon)	77.8	85.8	70.3
Intensity (s^{-1})	8000	3300	65

of segmentation of the germanium detectors is necessary to Doppler reconstruct the γ rays emitted by the nuclei in flight. The germanium detectors were arranged in two rings, at 37° and 90° with respect to the beam direction. For the ^{58}Ni and ^{56}Ni secondary beams a total of 15 detectors were in the setup, seven in the 37° ring and eight in the 90° ring. For the ^{54}Ni secondary beam 13 detectors were used, six in the 37° ring and seven in the 90° ring. The edge of the crystals of all detectors were at a distance of about 20 cm from the center of the gold target.

GEANT [19] simulations were performed for each observed γ-ray energy to determine the detector response. The Monte Carlo simulation was performed for ten million incident γ rays at each γ-ray energy, isotropically emitted in the projectile frame and Lorentz boosted with the beam velocity. The simulated histograms were fit with analytical curves to determine the expected peak shape as well as the area under the simulated peak, and thus the photopeak efficiency of the setup. These curves were then fit to the experimental spectra. The efficiency was further corrected for γ-ray angular distribution effects expected following Coulomb excitation.

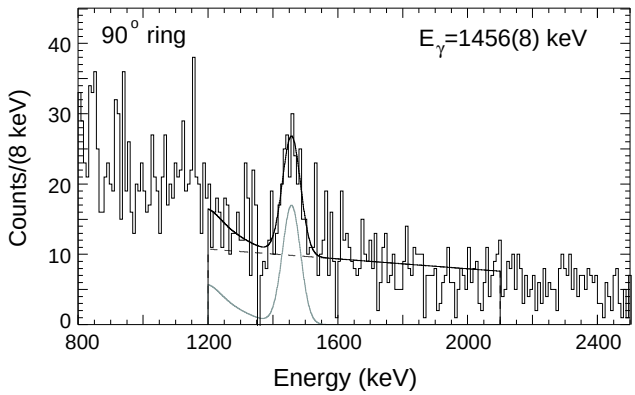

FIG. 1: Background-subtracted γ-ray spectrum for the 90° ring of SeGA in coincidence with ^{58}Ni particles ($\beta = 0.36$). The solid black line is the total fit, containing the sum of the scaled response function simulated in GEANT (grey line) and quadratic background (dashed line).

The γ–ray spectra shown in Fig. 1, 2 for ^{54,56,58}Ni were created for all nuclei satisfying the particle identification gates, with no restriction on the distance between target and

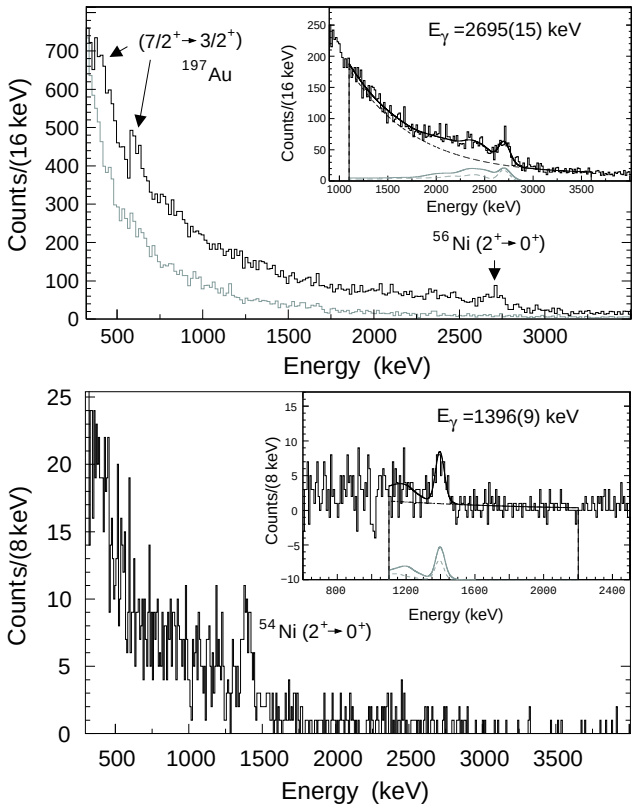

FIG. 2: Top panel: Projectile-frame ($\beta = 0.39$) γ-ray spectra in coincidence with ^{56}Ni. The spectrum in black was created with a software gate on the beam-related, prompt peak in the time spectrum, while the spectra in grey were obtained by cuts on the stationary background. The inset shows the projectile-frame spectrum with fits overlayed. Bottom panel: Projectile-frame ($\beta = 0.32$) γ-ray spectra in coincidence with ^{54}Ni particles. The background-subtracted projectile-frame spectrum is shown in the inset. For both panels the solid black line is the total fit, containing the sum of the simulated response functions for the 37° (solid grey line) and 90° (dashed grey line) rings on top of background (dot-dashed line).

projectile nuclei. As the minimum impact parameter is related to the laboratory scattering angle [21], the maximum laboratory scattering angles were chosen for each secondary beam (Table II) to restrict the impact parameter to at least the sum of the nuclear radii plus 2 fm. To extract the angle–integrated Coulomb excitation cross section σ for ^{58}Ni, a maximum scattering angle in the laboratory frame of $\theta_{lab}^{max} = 3.2°$ was chosen, corresponding to a minimum impact parameter b_{min} of 13.9 fm and thus a distance exceeding the sum of the nuclear radii of the target–projectile system by 2 fm. The resulting Coulomb excitation cross section of 175(36) mb translates into a $B(E2\uparrow)$ value of 707(145) e^2fm^4 using the Winther–Alder theory of relativistic Coulomb excitation [21]. In ^{58}Ni two 2^+ states at 3037 keV and 3263 keV with half-lives of 52(10) fs and 35(4) fs [22] are expected to be accessible via Coulomb excitation as well. The cross sections for the excitation of those states would be 21.0(35) mb and 32(4) mb, respectively. These comparably small cross sections and the low γ-ray detection efficiency at higher energies prevent the observation of the corresponding de-excitation γ rays in the spectrum (see Fig. 3, lower panel). From the branching ratios we can estimate that 7.2% and 7.3%, respectively, of the cross section

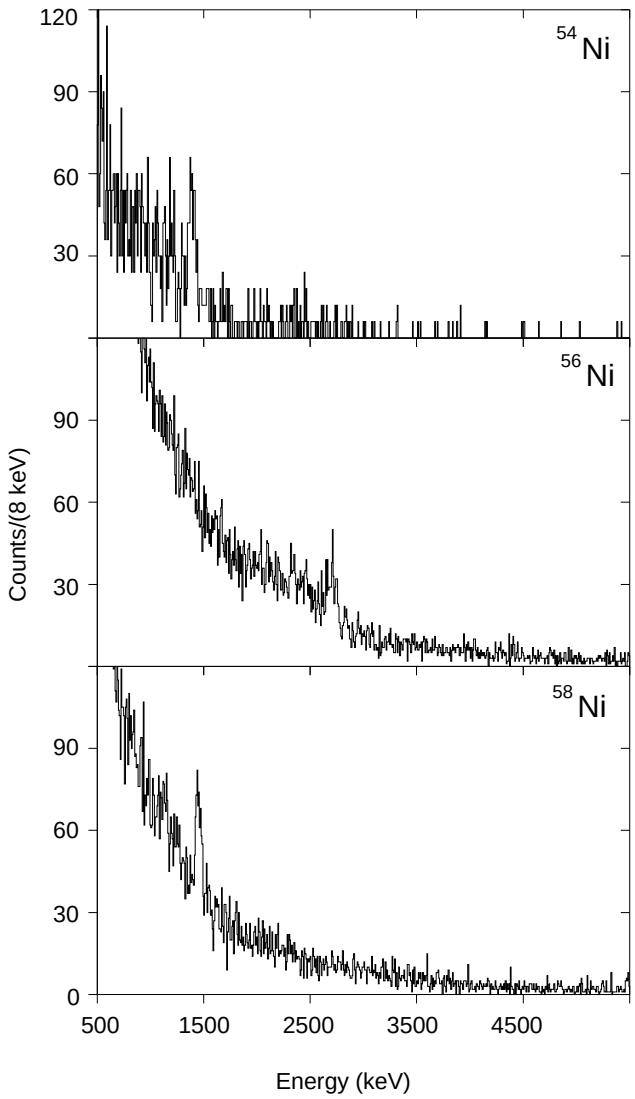

FIG. 3: γ-ray spectra from 500 to 5500 keV detected in coincidence with ^{54}Ni, ^{56}Ni and ^{58}Ni (sum of all detectors, no restrictions on the scattering angle). There is no clear experimental evidence for the excitation of higher-lying 2^+ states. The possibility of feeding is discussed in the text in great detail.

determined for the $0_1^+ \rightarrow 2_1^+$ excitation in ^{58}Ni might be due to feeding from those two levels. The cross section and $B(E2\uparrow)$ values corrected for the feeding are $\sigma = 150(34)$ mb and $B(E2\uparrow) = 605(139)\ e^2\mathrm{fm}^4$. The $B(E2\uparrow)$ value including the feeding corrections is in reasonable agreement with the adopted value of $695(20)\ e^2\mathrm{fm}^4$ [20]. The result without feeding correction is $B(E2\uparrow) = 707(145)\ e^2\mathrm{fm}^4$.

An upper limit of 6% from nuclear contributions to the Coulomb excitation cross section was estimated based on a calculation for the very similar reaction of ^{52}Fe scattered on ^{197}Au at 65 MeV/nucleon [18]. The ECIS88 coupled-channels code [23] was used with optical model parameters for ^{40}Ar scattering on ^{208}Pb at 41 MeV/nucleon [24] to calculate the contribution from nuclear excitations. We expect a similar contribution of at most 6% for the current measurements due to the similar mass and beam energies in the present experiments.

TABLE II: Gamma-ray energies, reaction kinematics, cross sections and $B(E2\uparrow)$ values for Coulomb excitation measurements performed in this work. Adopted values were taken from [20].

	^{58}Ni[a]	^{56}Ni	^{54}Ni
Experimental results			
E_γ (keV)	1453(8)	2695(15)	1396(9)
σ (mb)	175(36)	107(26)	134(36)
v/c (mid–target)	0.373	0.391	0.346
θ_{lab}^{max} (degrees)	3.2	2.9	3.5
b_{min} (fm)	13.9	14.3	16.2
$B(E2\uparrow)$ (e^2fm^4)	707(145)	494(119)	626(169)
Adopted values			
E_γ (keV)	1454.28(10)	2700.6(7)	–
$B(E2\uparrow)$ (e^2fm^4)	695(20)	600(120)	–

[a]corrected by the potential feeding from the 3037 keV and 3263 keV excited 2^+ states: $\sigma = 150(34)$ mb and $B(E2\uparrow) = 605(139)e^2$fm^4

The error on the Coulomb excitation cross section σ includes contributions from the statistical error on N_γ (between 5% and 12%) and N_{beam} ($< 1\%$), error on the measurement of the ^{197}Au target thickness ρ ($< 0.5\%$), and the error on the total photopeak efficiency (6%–12% depending on the energy of the de-excitation γ ray). The error on the reconstructed laboratory-frame scattering angle is 2 mrad FWHM ($\pm 0.05^\circ$) [16]. An additional error corresponding to the percentage difference in cross section for $\theta_{lab}^{max} - 0.05^\circ$ and $\theta_{lab}^{max} + 0.05^\circ$ was added to the total errors on the measured cross section and the reduced transition probability. The uncertainty quoted for the photopeak energy stems from the fit of the peak and a 0.5% systematic uncertainty attributed to the Doppler recontruction added in quadrature.

While a software gate applied on the appropriate scattering angle ensured the dominance of the electromagnetic interaction in the Coulomb excitation process of ^{58}Ni, it was not possible to employ the same method for ^{54}Ni or ^{56}Ni due to limited statistics and a low efficiency of the cathode-readout drift chambers used to reconstruct the laboratory scattering angle. Thus a method of scaling the measured cross section using the dependence of the ^{52}Fe cross section [18] on the laboratory scattering angle was developed.

^{52}Fe was present in the same cocktail beam as ^{54}Ni, and the higher rate and higher γ–ray efficiency at lower energies led to an accurate determination of the dependence of cross section on laboratory scattering angle [18]. Angle–integrated Coulomb excitation cross sections were calculated for maximum scattering angles of 1°, 2°, 3°, 3.5°, 4°, and 5°. The cross section with no scattering angle restriction was $\sigma_{\rm total} = 243(22)$ mb. A second-order polynomial was fit to the points between 2° and 3.5° to allow for interpolation. Using the second-order polynomial, the ^{52}Fe cross section was determined for each maximum scattering angle θ_{lab}^{max} listed in Table II. The maximum scattering angles for all nuclei studied were between 2.9° and 3.5°.

A cross section scaling factor S_θ for each maximum scattering angle was determined as $S_\theta = \sigma(\theta_{lab}^{max})/\sigma_{\rm total}$ using the ^{52}Fe data. Once cross sections with no scattering angle

restriction were determined for ^{54,56}Ni, multiplication by the appropriate S_θ resulted in the Coulomb excitation cross section σ. As the accuracy of the cross section determined using this method depends on the accuracy to which the ^{52}Fe cross section is measured, an additional percentage error was added to the cross section and $B(E2\uparrow)$ value measured for ^{54,56}Ni. The relative error on the ^{52}Fe total cross section of approximately 3%, which excludes the uncertainties on the SeGA efficiency and laboratory scattering angle, was included for all nuclei measured using this scaling method.

As a check of the scaling method, the Coulomb excitation cross section for ^{58}Ni was determined using this approach. A total cross section $\sigma_{\rm total} = 273(35)$ mb was measured. A scaling factor of $S_\theta = 0.66$ was determined for $\theta_{lab}^{max} = 3.2^\circ$ and multiplied by the total cross section. This resulted in a Coulomb excitation cross section of $\sigma = 180(34)$ mb, corresponding to $B(E2\uparrow) = 728(137)$ e^2fm^4 (the results are $\sigma = 150(31)$ mb and $B(E2\uparrow) = 622(128)$ e^2fm^4 with the feeding correction introduced earlier). The excitation cross section and $B(E2\uparrow)$ value determined using the scaling method are in good agreement with those determined with the 3.2° cut on the scattering angle. With the reasonable agreement between the measured Coulomb excitation cross section in the two methods for ^{58}Ni, this scaling method was used to determine the angle–integrated cross sections for ^{54,56}Ni.

The number of detected γ rays in coincidence with ^{56}Ni was determined from the fit shown in Fig. 2 (upper panel), and $\sigma_{\rm total} = 178(31)$ mb was the resulting cross section. A scaling factor of $S_\theta = 0.60$ was calculated for $\theta_{lab}^{max} = 2.9^\circ$, and multiplied by the total cross section for a result of $\sigma = 107(26)$ mb. With this Coulomb excitation cross section, $B(E2\uparrow) = 494(119)$ e^2fm^4 was determined.

The Doppler reconstructed γ–ray spectrum detected in coincidence with scattered ^{54}Ni shows a peak at 1396(9) keV (Fig. 2). The nature of intermediate–energy Coulomb excitation as well as $E(2_1^+) = 1408$ keV [25] in the mirror nucleus ^{54}Fe strongly suggests that the 1396 keV γ ray de–excites the 2_1^+ state of ^{54}Ni. A total cross section of 189(40) mb for ^{54}Ni was measured with the number of de-excitation γ rays determined using the fits from Fig. 2 (lower panel). With $S_\theta = 0.74$ calculated for $\theta_{lab}^{max} = 3.5^\circ$, an excitation cross section of 134(36) mb was extracted. A value of $B(E2; 0_1^+ \rightarrow 2_1^+) = 626(169)$ e^2fm^4 does result, a reduced transition probability very similar to the adopted value for the mirror nucleus ^{54}Fe of 640(13) e^2fm^4 [26].

Recent QRPA and diagonalization shell–model calculations [27] performed for $^{56-70}$Ni suggest that in the chain of Ni isotopes a significant amount of the total $B(E2\uparrow)$ strength can be distributed among higher–lying 2^+ states. For example, the small observed $B(E2; 0_1^+ \rightarrow 2_1^+)$ strength for ^{68}Ni was explained as due to fragmentation of the low–lying $E2$ strength into 2^+ states lying above 4 MeV, indicating that the energy splitting between the fp shell and the $g_{9/2}$ orbital is actually rather small and the low $B(E2\uparrow)$ cannot be explained by a possible restoration of the $N = 40$ harmonic oscillator magic number [27].

Unlike the case of ^{56}Ni, where the total $E2$ strength is predicted to be concentrated in the first 2^+ state, fragmentation is expected for ^{58}Ni [27]. The present experiment offers no evidence for the excitation of higher–lying 2^+ states in ^{58}Ni from the γ-ray spectra and a 14.5% overestimation of the measured $B(E2\uparrow)$ value by unobserved feeding into the 2_1^+ state has been calculated. The result is still in agreement with the adopted value quoted in [20].

The situation is more dramatic in ^{54}Ni, where the major fraction of the quadrupole collectivity of ^{54}Ni is expected in higher-lying 2^+ states according to shell-model calculations which will be discussed in the following. In fact, the present calculations predict the second

2^+ state to be more collective than the first 2^+ state. In light of these predictions and the rather low statistics in the ^{54}Ni experiment, unobserved feeding of the 2_1^+ state by the decays of the higher lying 2^+ states has to be considered carefully. In the following, the possible feeding contribution will be discussed in comparison to theory.

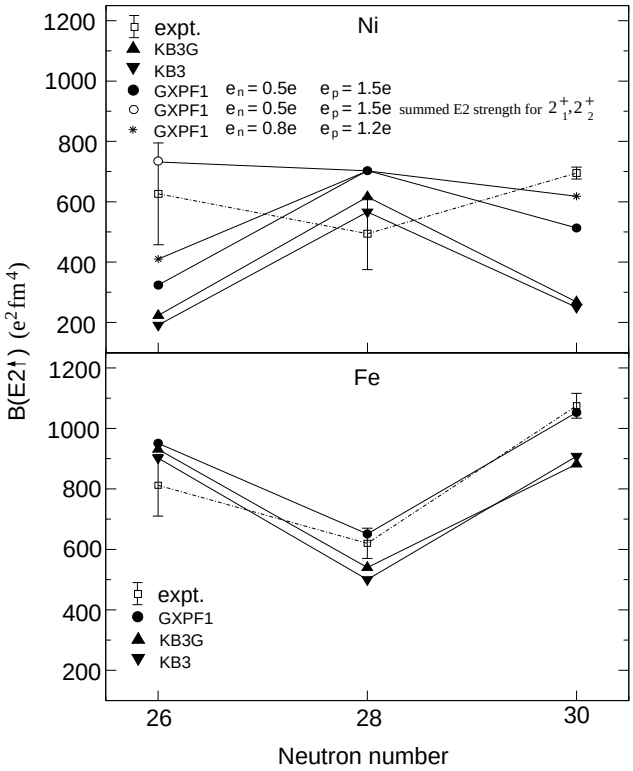

FIG. 4: Experimental $B(E2;0_1^+ \rightarrow 2_1^+)$ excitation strengths for the even–even Ni and Fe isotopes with neutron numbers $26 \leq N \leq 30$ are compared to large–scale conventional shell–model calculations using the KB3G [29], KB3 [30], and GXPF1 [31] effective interactions (code MSHELL [28] with $e_p = 1.5e$ and $e_n = 0.5e$). For the case of GXPF1 a calculation with the effective charges $e_p = 1.2e$ and $e_n = 0.8e$ is also given for the chain of Ni isotopes. Additionally, the experimental $B(E2\uparrow)$ given for ^{54}Ni is compared to the sum $B(E2;0_1^+ \rightarrow 2_1^+) + B(E2;0_1^+ \rightarrow 2_2^+)$ for the shell-model calculation using GXPF1 (see discussion in the text).

Large–scale conventional shell–model calculations (code MSHELL [28]) employing the KB3G [29], KB3 [30], and GXPF1 [31] effective interactions were performed for $^{54-58}$Ni as well as for the corresponding Fe isotones. For ^{54}Fe the GXPF1 [31] calculation gives [32] $B(E2;0_1^+ \rightarrow 2_1^+) = 651\ e^2\text{fm}^4$, $B(E2;0_1^+ \rightarrow 2_2^+) = 188\ e^2\text{fm}^4$ and $B(E2;0_1^+ \rightarrow 2_3^+) = 51\ e^2\text{fm}^4$, for states at 1.59, 2.97 and 3.23 MeV, respectively. These are in reasonable agreement with the experimental values of 640(13), 133(24) and 45(12) e^{2}fm^4 [26], respectively, for the 2^+ states at 1.408, 2.959 and 3.166 MeV, respectively. The KB3 (KB3G) results for ^{54}Fe are $B(E2\uparrow) = 500(540), 21(27), 236(240) e^2\text{fm}^4$ for 2^+ states at 1.61 (1.52), 3.86 (3.39), 4.63 (3.96) MeV, respectively. The GXPF1 results are in significantly better agreement with experiment for the second and third 2^+ states. The GXPF1 calculations for ^{54}Ni result in $B(E2;0_1^+ \rightarrow 2_1^+) = 324\ e^2\text{fm}^4$, $B(E2;0_1^+ \rightarrow 2_2^+) = 420\ e^2\text{fm}^4$ and $B(E2;0_1^+ \rightarrow 2_3^+) = 47\ e^2\text{fm}^4$. Thus the calculations predict a large mirror asymmetry in the $E2$ strength with the unusual prediction that most of the $E2$ strength in ^{54}Ni (55%) lies in

the 2_2^+ state. [The KB3 (KB3G) calculations gives 59% (54%) of the E2 strength to lie in the 3rd 2+ state of 54Ni].

There is only one clear peak in the ^{54}Ni γ–ray spectrum at an energy of 1.40 MeV. However, the energy ratio $E(2_2^+)/E(2_1^+) = 2.1$ in ^{54}Fe indicates the possibility that the transitions $2_2^+ \rightarrow 2_1^+$ and $2_1^+ \rightarrow 0_1^+$ in the mirror ^{54}Ni are degenerate within the limited γ–ray energy resolution in experiments with fast beams. We need to consider how this possible degeneracy could affect the interpretation of our data. [The spectrum in Fig. 2 indicates that the only peak–like structure (of about 10 counts) at higher energies appears at 2450 keV. If this corresponded to the 2_2^+ state, there would be a 500 keV shift from its mirror in ^{54}Fe much larger than any other displacement energy observed in this mass region.]

If we take the theoretical value of $B(E2; 0_1^+ \rightarrow 2_2^+) = 420\ e^2\text{fm}^4$ and a 50% decay branch to the 2_1^+ state as well as to the ground state as observed in the mirror nucleus, this would imply an overestimation of the Coulomb excitation cross section $\sigma(0_1^+ \rightarrow 2_1^+)$ and the resulting $B(E2\uparrow)$ value by 63%. A feeding–corrected $B(E2; 0_1^+ \rightarrow 2_1^+) = 230\ e^2\text{fm}^4$ would follow. However, within this scenario, a γ–ray peak with 12 counts would be expected at about 2.8 MeV in the spectrum displayed in Fig. 2 (lower panel). A peak with 12 counts between 2.7 and 2.9 keV can clearly be ruled out and an upper limit of less than 5 counts for a peak seems applicable in this energy region. Adjusting the decay branching ratio to the ground state and the 2_1^+ state so that 5 counts are to be in the peak corresponding to the ground–state transition would cause the peak at 1396 keV to be entirely due to feeding and the degeneracy of the $2_2^+ \rightarrow 2_1^+$ and $2_1^+ \rightarrow 0_1^+$ transitions. The possibility of no $E2$ strength in the 2_1^+ state is unlikely.

If the second 2^+ state has only half the excitation strength predicted, $B(E2; 0_1^+ \rightarrow 2_2^+) = 210\ e^2\text{fm}^4$, and the branching ratio is 50%, then the photo–peak at 2.8 MeV would have about 6 counts (consistent with the experimental limit) and 31% of the intensity in the peak at 1396 keV would be a result of the doublet structure with a corrected excitation strength $B(E2; 0_1^+ \rightarrow 2_1^+) = 428\ e^2\text{fm}^4$. Assuming a branching ratio of 25% to the ground state and 75% to the 2_1^+ level would reduce the experimental $B(E2\uparrow)$ value for the 2_1^+ state to $B(E2; 0_1^+ \rightarrow 2_1^+) = 333\ e^2\text{fm}^4$, which would be close to the shell–model prediction of $324\ e^2\text{fm}^4$. In this scenario, 3 counts would be expected in the $2_2^+ \rightarrow 0_1^+$ transition.

Given the possibility that the 2_2^+ state in ^{54}Ni lies at 2.9 MeV we conclude that our experimental excitation strength of 626(169) $e^2\text{fm}^4$ is most likely proportional to the sum $B(E2; 0_1^+ \rightarrow 2_1^+) + 2R \cdot B(E2; 0_1^+ \rightarrow 2_2^+) \approx B(E2; 0_1^+ \rightarrow 2_1^+) + B(E2; 0_1^+ \rightarrow 2_2^+)$ where R notes the branching ratio to the first excited 2^+ state and the factor 2 accounts for the potential doublet structure ($R = 0.5$ in the mirror nucleus ^{54}Fe). In Fig. 5 this is compared to the theoretical value for this sum. Accurate results for the individual ^{54}Ni $B(E2\uparrow)$ to all excited 2^+ states will require coincidence γ-ray data.

In Fig. 4 the $B(E2; 0^+ \rightarrow 2^+)$ values for ^{54,56,58}Ni are compared to the shell–model calculations described above. Additionally, the $B(E2\uparrow)$ values for the corresponding Fe isotones are given and compared to theory. These are $B(E2\uparrow)$ to the lowest 2^+ states except for ^{54}Ni for which we give the sum for 2_1^+ and 2_2^+ as discussed above. The truncation of the present calculation is $t = 6$ (six particles excited out of $f_{7/2}$) for ^{56}Fe and ^{58}Ni, and $t = 7$ for ^{54}Ni, ^{54}Fe, and ^{56}Ni. In the calculation for ^{52}Fe the excitations out of $f_{7/2}$ are not truncated. Effective charges $e_p = 1.5e$ and $e_n = 0.5e$ were used unless otherwise indicated. The experimental results for ^{54}Fe and ^{56}Fe are taken from [26, 33], with ^{52}Fe from [18]. The $B(E2\uparrow)$ quoted for ^{58}Ni is the adopted value from [20].

The theoretical pattern of $B(E2\uparrow)$ value is similar for all of the Hamiltonians. Overall

agreement for ^{52,54,56}Fe is good for all of the effective interactions with the best quantitative agreement obtained with GXPF1. With the energies of the 2^+ states for Fe at 0.850, 1.408 and 0.847 MeV, respectively, the product of $E_x B(E2)$ is approximately constant (Grodzins' rule [34]) as observed from global systematics and qualitatively described by collective models [20].

From ^{56}Ni to ^{58}Ni all of the calculations predict a drop in $B(E2\uparrow)$ in contrast to the experimental rise. Again GXPF1 is in best agreement with experiment. With the experimental energies of 2.700 MeV for ^{56}Ni and 1.454 MeV for ^{58}Ni, we find that experiment roughly obeys Grodzins' rule [34] whereas theory does not. The lowest 2^+ states in these two nuclei have very different structures, with ^{56}Ni being dominated the $f_{7/2} \rightarrow (p_{3/2}, f_{5/2})$ (ph) particle-hole excitations across the semi-magic shell $N = 28$, and ^{58}Ni being dominated by the $(p_{3/2}, f_{5/2})^2$ neutrons. For ^{58}Ni some of the $E2$ strength comes from mixing with the (ph) configuration. (Protons and neutrons have an effective charge that is related to the polarization of the core protons by the valence nucleons, described microscopically as a virtual coupling to the giant quadropole resonance [35].)

As discussed above, the data point for ^{54}Ni in Fig. 5 is for the sum of the lowest two 2^+ states. Theoretically these states have dominant components of two-holes (2h) and two-particles and four-holes (2p-4h) relative to a $(f_{7/2})^{16}$ configuration for ^{56}Ni. The second 2^+ state is part of a 4p-2h band. The division of the $E2$ strength between the lowest two 2^+ states is a signature of the configuration mixing between these two configurations. Determination of the division of strength will require a more sensitive experiment.

Most low-lying $E2$ transitions are isoscalar - that is, they have about equal proton and neutron components. Thus the isoscalar effective charge is well determined. For the calculations discussed above we use the conventional value of $e_p + e_n = 2.0e$ for the isoscalar effective charge. Near the semi-magic nucleus ^{56}Ni, the nuclei with two valence nucleons (^{54}Fe, ^{54}Ni, ^{58}Ni) have relatively large isovector components, for which the bare value of $e_p - e_n = 1.0e$ ($e_p = 1.5e$ and $e_n = 0.5e$) was used. However, since the average proton-neutron interaction is larger than the average proton-proton interaction, the polarization of the core protons is stronger for valence neutrons compared to valence protons. Thus we expect the amount added to the bare charge to be larger for neutrons than for protons [35]. To see this effect in the present comparisons we give the results obtained with e_p=1.2e and e_n=0.8e in the GXPF1 calculations for the Ni isotopes (Fig. 5). Some improvement is obtained for ^{58}Ni. But a wider systematic study of the $E2$ strength in this mass region is required to draw a firm conclusion on the isovector effective charge.

The results of the intermediate–energy Coulomb excitation measurements are summarized in Fig. 5. The characteristic rise in the energy of the first 2^+ state is rather predominant at $N = 28$ while the second signature for a shell closure, the expected minimum in the systematics of the $B(E2\uparrow)$ excitation strength, is less clear (see discussion above). The shell–model picture suggests a rather small fraction of the total $E2$ strength to be concentrated in the 2_1^+ state in ^{54}Ni, driven by fragmentation, similar to the mechanism that gives rise to the low $B(E2; 0_1^+ \rightarrow 2_1^+)$ value at the much discussed nucleus ^{68}Ni with $N = 40$. There is no solid evidence, however, for a strongly excited higher–lying 2^+ state in the present experiment on ^{54}Ni. The experimental $B(E2; 0_1^+ \rightarrow 2_1^+) = 626(169)$ e^2fm^4 is, in fact, closer to the total $B(E2\uparrow)_{\rm tot}$ value of 791 e^2fm^4 predicted within the shell–model calculation using the GXPF1 effective interaction.

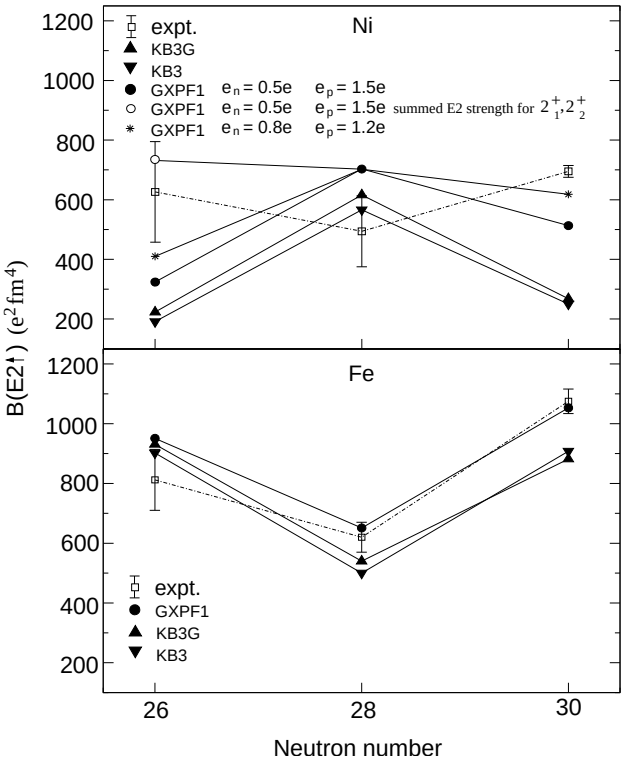

FIG. 5: Systematics of excitation energy and absolute $B(E2\uparrow)$ strengths for the first 2^+ state in the chain of Ni isotopes. Results from the present study are marked by open symbols. Other values are taken from [36–38] for $^{60-64}$Ni and from [12] for ^{66,68}Ni. The $B(E2\uparrow)$ for ^{54}Ni might be closer to the sum $B(E2;0^+_1 \rightarrow 2^+_1) + B(E2;0^+_1 \rightarrow 2^+_2)$ as discussed in the text.

Acknowledgments

We thank A. Stolz, T. Ginter, M. Steiner and the NSCL cyclotron operations group for providing the high–quality secondary and primary beams. This work was supported by the National Science Foundation under Grants No. PHY-0110253, PHY-9875122, PHY-0244453, INT-0089581 and in part by Grant-in-Aid for Specially Promoted Research (13002001) from the MEXT of Japan, and by the joint large-scale nuclear-structure calculation project by RIKEN and CNS.

[1] E. K. Warburton, J. A. Becker, and B. A. Brown, Phys. Rev. C **12**, 644 (1975).

[2] H. Scheit, T. Glasmacher, B. A. Brown , J. A. Brown, P. D. Cottle, P. G. Hansen, R. Harkewicz, M. Hellström, R. W. Ibbotson, J. K. Jewell, K. W. Kemper, D. J. Morrissey, M. Steiner, P. Thirolf, and M. Thoennessen, Phys. Rev. Lett. 77, 3967 (1996).

[3] T. Glasmacher, B. A. Brown, M. J. Chromik, P. D. Cottle, M. Fauerbach, R. W. Ibbotson, K. W. Kemper, D. J. Morrissey, H. Scheit, D. W. Sklenicka, and M. Steiner, Phys. Lett. **B 395**, 163 (1997).

[4] O. Sorlin *et al.*, Phys. Rev. C **47**, 2941 (1993).

[5] D. Sohler *et al.*, Phys. Rev. C **66**, 054302 (2002).

[6] N. Schulz, J. Chevallier, B. Haas, J. Richert, and M. Toulemonde, Phys. Rev. C **8**, 1779 (1973).
[7] G. Kraus *et al.*, Phys. Rev. Lett. **73**, 1773 (1994).
[8] Y. Yanagisawa *et al.*, AIP Conf. Proc. 455, 610 (1998).
[9] T. Motobayashi, Y. Ikeda, Y. Ando, K. Ieki, M. Inoue, N. Iwasa, T. Kikuchi, M. Kurokawa, S. Moriya, S. Ogawa, H. Murakami, S. Shimoura, Y. Yanagisawa, T. Nakamura, Y. Watanabe, M. Ishihara, T. Teranishi, H. Okuno, and R. F. Casten, Phys. Lett. **B 346**, 9 (1995).
[10] T. Glasmacher, Annu. Rev. Nucl. Part. Sci. **48**, 1 (1998).
[11] A. Gade, D. Bazin, C. M. Campbell, J. A. Church, D.-C. Dinca, J. Enders, T. Glasmacher, Z. Hu, K. W. Kemper, W. F. Mueller, H. Olliver, B. C. Perry, L. A. Riley, B. T. Roeder, B. M. Sherrill, and J. R. Terry, Phys. Rev. **C 68**, 014302 (2003).
[12] O. Sorlin et al., Phys. Rev. Lett. **88**, 092501 (2002).
[13] F. Marti, D. Poe, M. Steiner, J. Stetson, and X. Y. Wu, *Proc. 16th International Conference on Cyclotrons and Their Applications* (East Lansing, Michigan, 2002).
[14] D. J. Morrissey, B. M. Sherrill, M. Steiner, A. Stolz, and I. Wiedenhöver, Nucl. Instrum. Methods in Phys. Res. B **204**, 90 (2003).
[15] W. F. Mueller, J. A. Church, T. Glasmacher, D. Gutknecht, G. Hackman, P. G. Hansen, Z. Hu, K. L. Miller, and P. Quirin, Nucl. Instrum. Methods in Phys. Res. **A 466**, 492 (2001).
[16] J. Yurkon, D. Bazin, W. Benenson, D. J. Morrissey, B. M. Sherrill, D. Swan, and R. Swanson, Nucl. Instrum. Methods in Phys. Res. **A 422**, 291 (1999).
[17] D. Bazin, J. A. Caggiano, B. M. Sherrill, J. Yurkon, and A. Zeller, Nucl. Instrum. Methods in Phys. Res. B **204**, 629 (2003).
[18] K. L. Yurkewicz, D. Bazin, B. A. Brown, C. M. Campbell, J. A. Church, D.-C. Dinca, A. Gade, T. Glasmacher, M. Honma, T. Mizusaki, W. F. Mueller, H. Olliver, T. Otsuka, L. A. Riley, and J. R. Terry, Phys. Rev. **C**, accepted for publication.
[19] GEANT–detector description and simulation tool, version 3.21, Technical Report W5013, CERN (1994).
[20] S. Raman, C. W. Nestor, Jr., and P. Tikkanen, At. Data and Nucl. Data Tables **78**, 1 (2001).
[21] A. Winther and K. Alder, Nucl. Phys. **A319**, 518 (1979).
[22] B. Singh and M. R. Bhat, Nucl. Data Sheets **80**, 789 (1997).
[23] J. Raynal, Phys. Rev. C **23**, 2571 (1981).
[24] T. Suomijärvi, D. Beaumel, Y. Blumenfeld, Ph. Chomaz, N. Frascaria, J. P. Garron, J. C. Roynette, J. A. Scarpaci, J. Barrette, B. Fernandez, J. Gastebois, and W. Mittig, Nucl. Phys. **A509**, 369 (1990).
[25] M. R. Bhat, Nucl. Data Sheets **86**, 315 (1999).
[26] H. Junde, Nucl. Data Sheets **68**, 887 (1993).
[27] K. Langanke, J. Terasaki, F. Nowacki, D. J. Dean, and W. Nazarewicz, Phys. Rev. C **67**, 044314 (2003).
[28] T. Mizusaki, RIKEN Accel. Prog. Rep. **33**, 14 (2000).
[29] A. Poves *et al.*, Nucl. Phys. **A694**, 157 (2001).
[30] A. Poves and A. P. Zuker, Phys. Rep. **70**, 235 (1981).
[31] M. Honma, T. Otsuka, B. A. Brown, and T. Mizusaki, Phys. Rev. C **65**, 061301 (2002).
[32] M. Honma, T. Otsuka, B. A. Brown, and T. Mizusaki, Phys. Rev. C **69** (2004) in press.
[33] H. Junde, Nucl. Data Sheets **89**, 315 (1999).
[34] L. Grodzins, Phys. Lett. **2**, 88 (1962).
[35] B. A. Brown, A. Arima, and J. B. McGrory, Nucl. Phys. **A277**, 77 (1977).

[36] J. K. Tuli, Nucl. Data Sheets **100**, 347 (2003).
[37] H. Junde and B. Singh, Nucl. Data Sheets **91**, 317 (2000).
[38] B. Singh, Nucl. Data Sheets **78**, 395 (1996).